Spatial variability of diurnal to seasonal cycles of precipitation from a high-altitude equatorial Andean valley to the Amazon Basin

Jean-Carlos Ruiz-Hernández, Thomas Condom, Pierre Ribstein, Nicolas Le Moine, Jhan-Carlo Espinoza, Clementine Junquas, Marcos Villacís, Andrea Vera, Teresa Muñoz, Luis Maisincho, et al.

Journal of Hydrology: Regional Studies 38 (2021) 100924

Contents lists available at ScienceDirect

Journal of Hydrology: Regional Studies

journal homepage: www.elsevier.com/locate/ejrh

Spatial variability of diurnal to seasonal cycles of precipitation from a high-altitude equatorial Andean valley to the Amazon Basin

Jean-Carlos Ruiz-Hernández [a,b,*], Thomas Condom [b], Pierre Ribstein [a], Nicolas Le Moine [a], Jhan-Carlo Espinoza [b], Clementine Junquas [b], Marcos Villacís [c], Andrea Vera [d], Teresa Muñoz [e], Luis Maisincho [f], Lenin Campozano [c], Antoine Rabatel [b], Jean-Emmanuel Sicart [b]

[a] Sorbonne Université, UMR 7619 METIS, Case 105, 4 place Jussieu, F-75005, Paris, France
[b] Univ. Grenoble Alpes, IRD, CNRS, Grenoble INP, Insitut des Géosciences de l'Environnement (IGE, UMR 5001), 38000, Grenoble, France
[c] Escuela Politécnica Nacional (EPN), Departamento de Ingeniería Civil y Ambiental, Quito, 170525, Ecuador
[d] Fondo para la Protección del Agua (FONAG), Quito, Ecuador
[e] Empresa Pública Metropolitana de Agua Potable y Saneamiento (EPMAPS-Agua de Quito), Quito, 17-03-0330, Ecuador
[f] Instituto Nacional de Meteorología e Hidrología (INAMHI) Iñaquito N36-14 y Corea, Quito, Ecuador

ARTICLE INFO

Keywords:
Precipitation variability
Diurnal and seasonal cycles
Equatorial Andes

ABSTRACT

Study region: The upper part of the Guayllabamba and Napo basins (78.2 ° W, 0.3 °S; 18,500 km^2) in the equatorial Andes, which are vulnerable to stress on the ecosystem services.
Study focus: This paper analyses the diurnal cycle of precipitation over a transect from the Andes to the Amazon. The diurnal cycle is estimated as the diurnal distribution of precipitation for 2014–2019 using records from 80 stations. Cluster analysis performed on the diurnal cycle estimates depicts the spatial association between the diurnal and seasonal cycles of precipitation.
New hydrological insights: A northwest-southeast spatial variation in the diurnal and seasonal cycles is identified with four groups of stations. In the western part, the seasonal cycles of Groups 1 and 2 are bimodal with precipitation maxima in the March-April and October-November seasons and a short drier season in July-August. In the eastern part, Group 3 also presents bimodality, but a weaker seasonal cycle. Conversely, Group 4 is unimodal with a peak in June. Distinct diurnal cycles are observed in both drier and wetter seasons of Groups 1–3; no marked diurnal cycle is observed in Group 4. Groups 3 and 4 are the most spatially heterogeneous, with an exceptional horizontal variation of 330 mm/yr/km. The analysis of these variations provides insight into the atmospheric dynamics driving precipitation in this zone, and may help to better optimize the water supply system.

* Corresponding author.
E-mail addresses: jeanka1991@hotmail.com (J.-C. Ruiz-Hernández), thomas.condom@ird.fr (T. Condom), pierre.ribstein@sorbonne-universite.fr (P. Ribstein), nicolas.le_moine@upmc.fr (N. Le Moine), jhan-carlo.espinoza@ird.fr (J.-C. Espinoza), clementine.junquas@univ-grenoble-alpes.fr (C. Junquas), marcos.villacis@epn.edu.ec (M. Villacís), andrea.vera@fonag.org.ec (A. Vera), teresa.munioz@aguaquito.gob.ec (T. Muñoz), lmaisincho@inamhi.gob.ec (L. Maisincho), lenin.campozano@epn.edu.ec (L. Campozano), antoine.rabatel@univ-grenoble-alpes.fr (A. Rabatel), jean-emmanuel.sicart@ird.fr (J.-E. Sicart).

https://doi.org/10.1016/j.ejrh.2021.100924
Received 26 November 2020; Received in revised form 28 August 2021; Accepted 15 September 2021
Available online 25 October 2021

1. Introduction

The diurnal cycle is the finest-scale regular mode of precipitation variability and is an essential aspect of local climate and the hydrological cycle. The diurnal cycle results from the interplay between regional mechanisms and complex local atmospheric circulations induced by topography and land-atmosphere interactions, and is driven mainly by the marked diurnal amplitude of temperature (Yang and Slingo, 2001; Takahashi et al., 2010; Junquas et al., 2018; Kumar et al., 2020; Espinoza et al., 2020). Precipitation variations become much more complex in mountainous regions, where the topography induces strong horizontal and altitudinal gradients (e.g. Immerzeel et al., 2014; Guo et al., 2014; Espinoza et al., 2015; Chavez and Takahashi, 2017), defining not only diurnal but also contrasted seasonal modes of variability (e.g. Oettli and Camberlin, 2005; Takahashi, 2010; Ilbay-Yupa et al., 2021).

In the Andean region, previous studies used datasets from precipitation stations, highlighting the role of the rough topography in modulating the diurnal cycle of precipitation. In the northern Andes (1 °N-11 °N; Colombia), Poveda et al. (2005) used 51 rainfall stations to reveal the heterogeneity of the diurnal cycle even between nearby stations, attributing these changes to the interplay of topography with synoptic and local-scale circulations. More recent research conducted in the Medellin Andean valley (6 ° N-6.6 ° N; Colombia) shows that the diurnal cycle is spatially *coherent* and varies seasonally depending on the life cycle of deep and large convective systems modulated at diurnal time scales (Bedoya et al., 2019). In the current study, the term *coherence* is also used to describe a common spatial behaviour of precipitation at different time scales (diurnal and seasonal).

The diurnal cycle of precipitation is often used to test physical parameterisations in atmospheric models since its representation is difficult (Junquas et al., 2018; Konduru and Takahashi, 2020). Junquas et al. (2018) analysed the diurnal cycle of precipitation in the Central Andes (13 °S-17 °S; Peru) via mesoscale atmospheric modelling, suggesting that thermally driven, local-scale diurnal circulation patterns control the diurnal precipitation cycle. The latter mechanism triggers winds that transport moisture upslope during the day and downslope at night. A mechanical channelisation of upslope moisture transport is also described during the day along the eastern Andean valleys.

The sparsity and uneven distribution of networks of meteorological stations in mountain environments make characterising precipitation a challenging task (Buytaert et al., 2006; Padrón et al., 2015; Condom et al., 2020). Particularly, long-term hourly records are rare or non-existent in most of the equatorial Andes due to the harsh environmental conditions. The advances in remote sensing techniques (e.g., satellite retrievals, radar profiles) have significantly contributed to better characterisation of the diurnal cycle over tropical south America (e.g. Negri et al., 2000, 2002; Mapes et al., 2003; Giles et al., 2020). However, studies related to the tropical Andes are either limited by short observation periods or coarse spatial resolution of satellite retrievals (e.g. Bendix et al., 2006a; Campozano et al., 2016; Ballari et al., 2018; Campozano et al., 2018). For instance, Bendix et al. (2006b) examined the diurnal cycle of precipitation in a southern Ecuadorian Andes-Amazon valley (oriented west to east) using a Doppler rain-radar profiler to recognise two diurnal rainfall maxima peaking around sunrise (05:30−06:30 LT) and in the early afternoon (14:30−15:30 LT). The first peak is attributed to mesoscale convective systems (MCS) developed during the nighttime over the Amazon plains and extending toward the Andes by mid-level easterlies, and the second one to local thermally-driven convection. Furthermore, thermally driven upslope flow contributes to cloud formation in the eastern Cordillera range releasing rainfall during the day that can also reach the inter-Andean valleys. MCS are more frequent during the night, and their size remains constant throughout the year, regardless of their seasonal cycle (Campozano et al., 2018). It can be concluded from the literature that the diurnal cycle displays an afternoon-evening peak in Andean valleys and a midnight-dawn peak in the Andes-Amazon slopes.

Precipitation variability in many cases is the major source of uncertainty in catchment hydrology (e.g., Beven, 2012; Buytaert et al., 2006). This is especially true in the high-altitude environments of the tropical Andes that provide essential ecosystem services like water storage and streamflow regulation for downstream water uses (González-Zeas et al., 2019). Andean catchments, particularly those covered by Páramo (i.e. a high altitude neotropical grassland ecosystem), respond quickly (< 24 h) to storm precipitation events producing flash-floods that cause human losses and damages to water supply systems (Muñoz et al., 2018). In addition, partially glacierized catchments (> 5000 m asl. approx.) undergo continuous ablation and accumulation processes at sub-daily time scales throughout the year (Favier et al., 2004). Recently, seasonal and west-east spatial variations of the Normalized Difference Vegetation Index (NDVI) have been identified in the Ecuadorian Andes and greening peaks are generally associated with lower rainfall (Haro-Carrión et al., 2021). To investigate such processes, fundamental knowledge about the diurnal variability of precipitation is required.

Thus, this paper aims to examine the spatial variability of precipitation in the Andes-Amazon transition zone of Ecuador in order to give insights to investigate atmospheric dynamics driving the diurnal cycle and support water management. To that goal, the coherence of diurnal and seasonal cycles of precipitation and its relationship with the topography is analysed thanks to a unique dataset from a dense stations network. Specifically, the paper tackles the concomitant spatial variation of both diurnal and seasonal cycles that has not been reported yet by previous studies in the region. The target domain is a rectangular zone in the equatorial Andes of 18,500 km^2 with an altitude between 400 and 5,750 m a.s.l. This region shows high vulnerability to suffering stress on the ecosystem services due to the progressive increase of the population and urgently requires new strategies for water management.

2. Materials and methods

2.1. Study area and climate settings

The study zone (78.2 ° W, 0.3 °S) encompasses the upper Guayllabamba Basin and the upper Napo Basin draining, respectively, to the Pacific and Amazonas basins. It extends over 18,500 km^2 and is characterized by steep slopes with an altitude between 400 and

5,750 m a.s.l. (Fig. 1b). This zone is critical because it hosts a vast and currently expanding water infrastructure that supplies water for human consumption in Quito, the capital of Ecuador, and other surrounding urban areas (González-Zeas et al., 2019). The Andes Cordillera in the zone exhibits a predominant NE-SW orientation and branches into two major mountain ranges, the so-called Cordillera Occidental (western branch) and Cordillera Central (eastern branch), both characterized by volcanoes and some summits covered by glaciers (Fig. 1b). The annual precipitation in the inter-Andean valley varies from 400 mm/yr in the bottom of the valley and reaches 1500 mm/yr on the flanks of the Cordillera (Pouget et al., 2017). Conversely, the upper Napo Basin displays heterogeneous annual precipitation ranging from 1000 mm/yr on the Cordillera Central ridges and reaching up to 6000 mm/yr on the Andes-Amazon foothills (Laraque et al., 2007). Indeed, similar heterogeneity in the amount of annual precipitation has been observed along the tropical Andes-Amazon slopes (5 °N-20 °S) (e.g. Espinoza et al., 2009, 2015; Halladay et al., 2012; Chavez and Takahashi, 2017; Kumar et al., 2020; Saavedra et al., 2020).

The moisture barrier effect of the Andes modulates the precipitation regimes on the Pacific and Amazon sides at multiple time

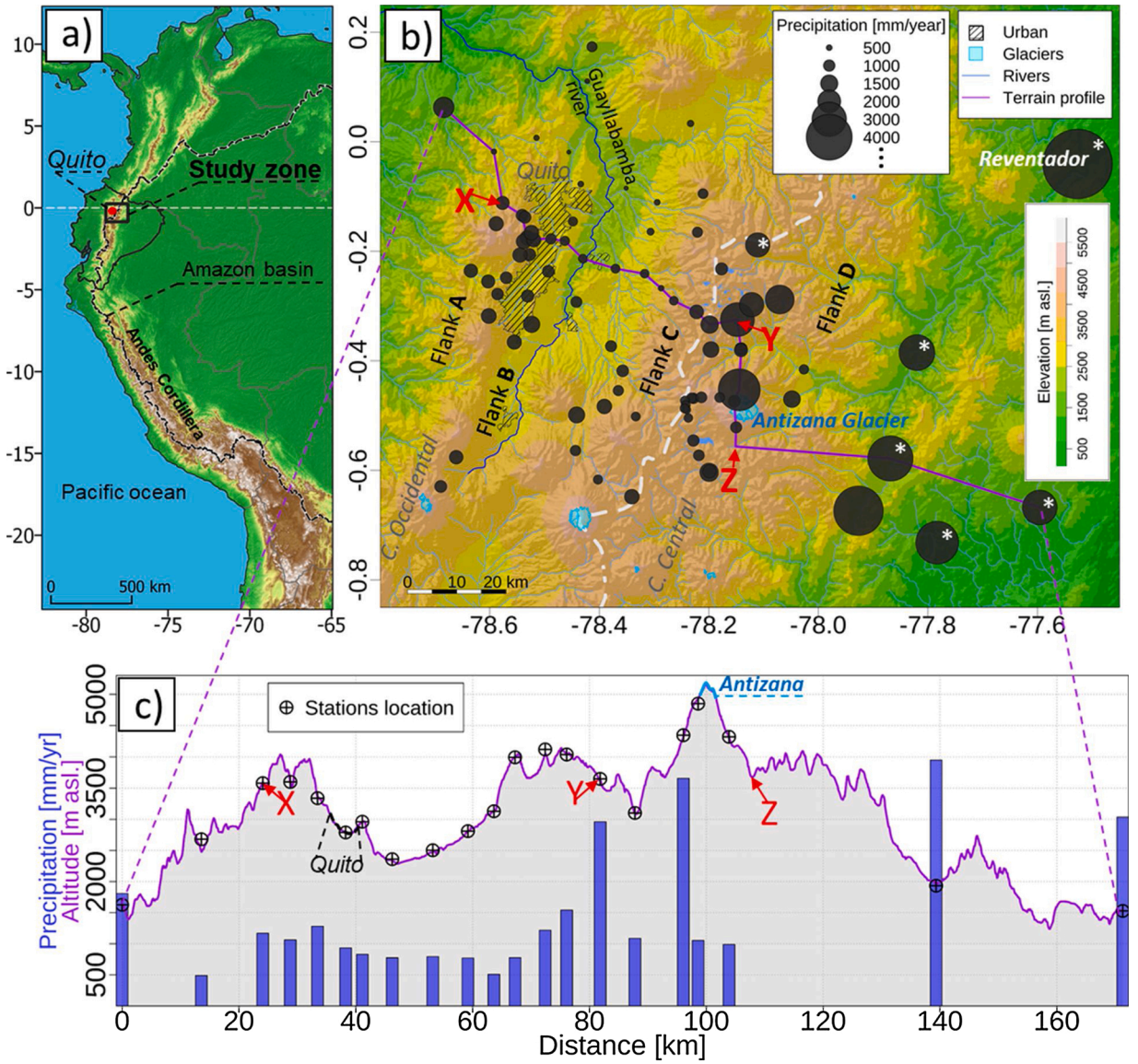

Fig. 1. a) Location of the study zone in the equatorial Andes. The topography of the Andes is represented using SRTM data. b) Topography configuration of the study zone and spatial distribution of the mean annual precipitation measured by 80 (hourly data) and six (monthly data, white stars) stations over the 2014–2019 period. The white dashed line is the upper limit of the Napo Basin, and the brown line delineates the Guayllabamba Basin. The Guayllabamba River represents the talweg of the inter-Andean valley to delineate Flanks A-D on the Cordillera. The topography is represented using a Digital Elevation Model at a resolution of 100 m provided by the Instituto Gegráfico Militar (IGM-Ecuador). The city of Quito and urban areas larger than 5 km^2 are also indicated. c) Topographical NW-SE profile (purple line) and mean annual precipitation for selected stations (blue bars). Points X, Y and Z are geographical references used to describe the profile.

scales, which interact on the regional to local spatial scales (Campozano et al., 2018; Espinoza et al., 2020). The inter-annual variability of precipitation is in part modulated by anomalies in the sea surface temperature of the tropical Pacific and Atlantic oceans (Vuille et al., 2000). Among them, the El Niño Southern Oscillation (ENSO) produces positive precipitation anomalies that are responsible for several socio-economic impacts on equatorial Andean populations (e.g. Vuille et al., 2000; Rossel and Cadier, 2009; Vicente-Serrano et al., 2017). In addition, the Madden-Julian Oscillation (MJO) drives the intra-seasonal precipitation variability in Ecuador (Recalde-Coronel et al., 2020).

The Intertropical Convergence Zone (ITCZ) meridional migration partly modulates precipitation seasonality and inter-annual extremes (Segura et al., 2019). The northern Pacific Slope region is influenced by moisture transported upslope from the eastern Pacific during the December-May season, associated with the southward displacement of the ITCZ (Vázquez-Patiño et al., 2020). In the plains along the Ecuadorian coast, the seasonal cycle of precipitation is generally unimodal with a peak during austral autumn (Bendix and Lauer, 1992; Vicente-Serrano et al., 2017), corresponding to the southernmost position of the eastern Pacific ITCZ during a normal year (Mitchell and Wallace, 1996; Garreaud, 2009).

On the other hand, in the eastern part of the Andes, a different unimodal rainfall regime is observed with a peak during austral winter, associated with the advection of water vapour from the Amazon Basin by enhanced easterlies during this season. In addition, a bimodal seasonal cycle, peaking around March-May and October-November, is documented in the inter-Andean valleys, which is characterized by dry conditions during austral winter related to strong atmospheric subsidence (Campozano et al., 2016; Segura et al., 2019). Consequently, only one rainy season (December-May) occurs in the coastal plains, with one or two rainy seasons (June-July or March-May and October-November) in the inter-Andean valleys and Amazon plains (e.g. Bendix and Lauer, 1992; Laraque et al., 2007; Espinoza et al., 2009; Garreaud, 2009; Campozano et al., 2016; Vicente-Serrano et al., 2017). Two other large-scale phenomena are associated with the seasonality of precipitation: the east Andean low-level jet (LLJ); and the development of mesoscale convective systems that exhibit varying diurnal features (e.g. Marengo, 2002; Rollenbeck and Bendix, 2011; Montini et al., 2019)

2.2. Hydroclimatic data

2.2.1. Precipitation data

Rainfall data for the study site are provided at an hourly time step by three local manager institutions: the *Empresa Pública Metropolitana de Agua Potable y Saneamiento* (EPMAPS), the *Fondo para la Protección de Agua* (FONAG), the *Instituto Nacional de Meteorología e Hidrología* (INAMHI) and the French National Observation Service (GLACIOCLIM, *Les GLACiers, un Observatoire du CLIMat*) which meticulously collect, process, and check the precipitation records following the protocols suggested by the World Meteorological Organization (WMO) (WMO, 2007, 2015). Data from a total of 130 stations (1 GLACIOCLIM, 23 INAMHI, 34 FONAG and 72 EPMAPS stations), all with tipping bucket rain gauges (with an accuracy of 0.2 mm per tip), were compiled. The data quality and data availability over the 2014–2019 study period were checked in this study to estimate the diurnal cycle, thereby reducing the amount of data to 80 rainfall stations (Table S1, Supplementary Material). Only the stations that meet the following conditions were retained: 1) a maximum of 20 % data gaps in the entire study period; and 2) Data for any given month must be available during a minimum of four years, again using a data gap threshold of 20 %. One exception is made to the criteria: six stations with scarce monthly precipitation values located on the Amazonian flank (white stars in Fig. 1b) were included in order to use data from these remote areas that are characterized by scarce information and a lack of knowledge. Notice that only the 80 hourly rainfall stations are used to estimate the diurnal cycle (Fig. 1b).

2.2.2. Atmospheric data

Seasonal atmospheric circulation was analysed using both meridional and zonal winds at 850 hPa from the European Centre for Medium-Range reanalysis ERA5 (Hersbach et al., 2020) for the 2014–2019 period. The 850 hPa winds (u and v in m s^{-1}) are highly relevant to properly describing the atmospheric circulation in South America (e.g. Espinoza et al., 2009, 2012; Paccini et al., 2017). Furthermore, low-level winds are the major drivers of precipitation variability in the Andes-Amazon transition region since they transport most of the moisture towards the Cordillera (Vázquez-Patiño et al., 2020; Figueroa et al., 2020).

Conversely, diurnal circulation was analysed using hourly-monthly means also from ERA5 during 2014–2019. The selected months were January, April, July, and October because they are the middle month of each season. Additionally, the hours 14h00 LT and 02h00 LT were selected in order to contrast daytime with nighttime circulations. These hours agree with the initiation of precipitation maxima in the daytime (locally induced) and nighttime (regionally induced) convection in the zone (Bendix et al., 2006b; de Angelis et al., 2004). The vertical structure of the atmosphere is also described using zonal winds (u in m s^{-1}), the vertical velocity Omega (w in Pa s^{-1}) and the specific humidity (q in g kg^{-1}) from 1000 hPa to 300 hPa.

2.3. Diurnal cycle estimation

To avoid effects of large differences in the amount of precipitation between stations (e.g., in the Amazon plain vs the Andean stations), we estimated the diurnal cycle (%) as the percent of total daily rainfall instead of the traditional diurnal cycle expressed in terms of precipitation intensity (mm/h). Hourly precipitation data was used to estimate the diurnal cycle associated with each station following the formulation published in the literature (e.g., Oki and Musiake, 1994; Poveda et al., 2005; Bedoya et al., 2019) that states that the diurnal cycle DC1 (%) can be defined by:

$$DC1_{m,h} = \frac{P_{m,h}}{\frac{1}{24}\sum_{h'=0}^{23} P_{m,h'}} \times 100 \quad (1)$$

where $P_{m,h}$ (mm/h) is the long-term (2014–2019) average of precipitation measured in the time interval $]h-1,h]$ of the hour h in the month m. The index h in Eq. (1) refers to hours (00−23 h LT). $DC1_{m,h}$ (Eq. (1)) can be interpreted as the normalized diurnal cycle of each month or the anomaly (%) of the precipitation at hour h in month m of the year (Oki and Musiake, 1994). For clustering purposes and to correct for the non-concordance between the peak hours of the diurnal cycle at the nearby stations (e.g., Poveda et al., 2005), we also calculated the diurnal cycles DC3 (%) at 3h and DC6 (%) at 6h time-steps through the aggregation of $DC1_{m,h}$ as follows:

$$DC3_{m,h=3\times i} = \sum_{h=3\times i}^{3\times i+2} DC1_{m,h} \quad (2)$$

$$DC6_{m,h=6\times i} = \sum_{h=6\times i}^{6\times i+5} DC1_{m,h} \quad (3)$$

where $i = 0, \ldots, 7$ for DC3 and $i = 0, \ldots, 3$ for DC6. This means that DC3 is the sum of the diurnal cycle DC1 every three hours starting at 00, 03, 06, 09, 12, 15, 18 and 21 h LT. Similarly, DC6 is the sum of the diurnal cycle DC1 every six hours starting at 00, 06, 12, and 18 h LT. The definitions of diurnal cycle according to Eqs. (1)–(3); generate respectively three different datasets of diurnal cycle estimations: the 1h-, 3 h- and 6 h-dataset (Fig. S-1). Each dataset has 80 members (diurnal cycles) and is used in cluster analysis in order to find dominant modes of diurnal variability in the zone. It is assumed that the six years of hourly data used in this study is sufficient to capture the diurnal and seasonal variations of precipitation (e.g. Bedoya-Soto et al., 2019) since these modes of variability are regular and closely periodic over time (Espinoza et al., 2020; Arias et al., 2021).

2.4. Cluster analysis

To detect dominant diurnal cycles and delineate their associated groups, we used the unsupervised "partitioning around medoids" (PAM) clustering method where dissimilarity measures and a number of groups k must be specified in order to cluster the datasets (Kaufman and Rousseeuw, 2008). PAM is a k-medoid based algorithm but uses data points as centers (real members or stations) instead of a centroid (non-observable mean) representative of a group. Specifically, its advantage relies on the medoid, a true spatially localizable station, which can describe the diurnal cycle groups through only one observed diurnal cycle.

The chosen measure of dissimilarity to be minimized in PAM is the Manhattan distance, which is based on the absolute distance between members and diminishes the influence of unusual values (outliers), which can exaggerate dissimilarities such as in Euclidean distances. Clustering methods have been widely used to regionalize rainfall patterns, as demonstrated in several studies (e.g. Oki and Musiake, 1994; Rau et al., 2016; Trachte et al., 2018). A more detailed description of PAM can be found in Trachte et al. (2018).

The number of groups k was selected using the gap statistic that compares the change in within-cluster dispersion with that expected under an appropriate null distribution (Tibshirani et al., 2001). We analysed feasible k groups between 2 and 10 suggested by the gap statistic for each diurnal cycle dataset (1h-, 3 h-, and 6 h-dataset). Inspecting visually the spatial pattern displayed over topography and the representation of groups in the principal components space PC1-PC2, we chose both the *dataset* and k hat do not permit the groups' convex hulls to overlap in the PC1-PC2 space.

2.5. Seasonality assessment

With the aim to understand whether precipitation diurnal cycle groups are related to seasonality, we calculated the seasonal index (SI) suggested by Walsh and Lawler (1981) for each precipitation station as follows:

$$SI = \frac{1}{\widehat{R}} \sum_{m=1}^{12} \left| \widehat{x_m} - \frac{\widehat{R}}{12} \right| \quad (4)$$

where $\widehat{R}$ is the mean annual precipitation and $\widehat{x_m}$ is the mean monthly precipitation of month m. Table 1 shows the qualitative classification of degrees of seasonality.

Table 1
Seasonality index classes according to Eq. (4) (Walsh and Lawler, 1981).

Rainfall regime	SI Class limits
Very Equable	£ 0.19
Equable but with a definite wetter season	0.20−0.39
Rather seasonal with a short drier season	0.40−0.59
Seasonal	0.60−0.70
Markedly seasonal, with a longer drier season	0.80−0.99
Most rain in 3 months or less	1.00−1.19

3. Results

3.1. Spatial pattern of annual precipitation

A clear contrast is observed between precipitation in the inter-Andean valley in the Guayllabamba Basin (Flanks A, B and C in

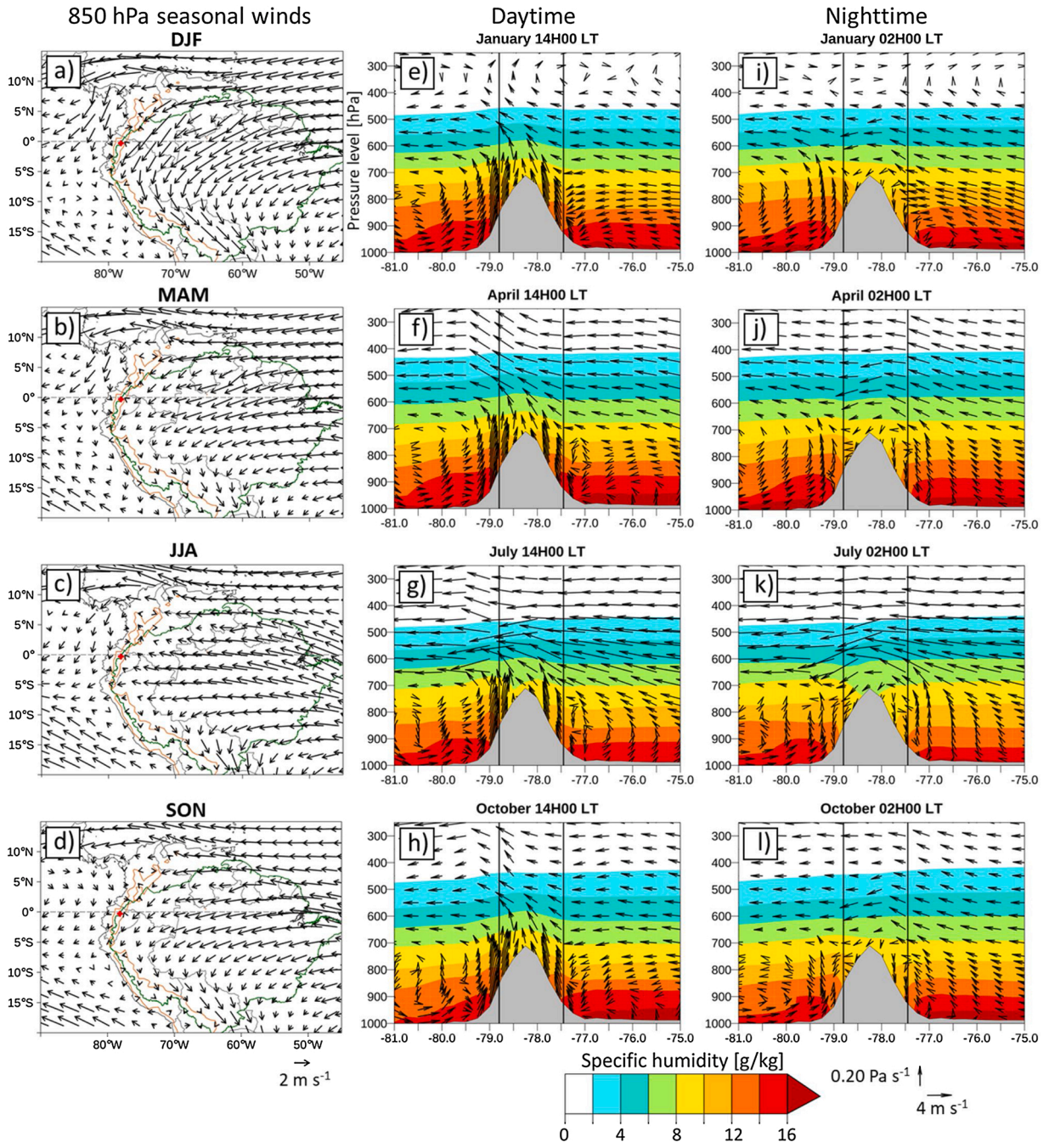

Fig. 2. Seasonal and diurnal circulations during 2014–2019. Mean seasonal horizontal winds at 850 hPa during a) December-February (DJF), b) March-May (MAM), c) June-August (JJA), and d) September-November (SON). The brown line represents the Andes elevation at 1500 m a.s.l.), and the green line is the Amazon basin. In a)–d), the study zone is indicated by a red dot. Pressure-longitude cross-section of the zonal-vertical mean of wind velocity (vectors) and mean specific humidity (shaded) for selected hours in e)–h) daytime and i)–l) nighttime during the middle month of each season. In e)–l), the vertical black lines enclose the study zone, and the grey shaded area is the topography according to ERA5. The meridional mean in cross sections were computed over the extend (−81 °W, -75 °W; 0.75 °S, 0.25 ° N).

Fig. 1b) and on the Amazonian slopes (Flank D in Fig. 1b). In the inter-Andean valley, the lowest precipitation values are observed in the surroundings of the valley's talweg, decreasing to 400 mm/yr, whereas the flanks of the Cordillera show higher precipitation values up to approximately 1,200 mm/yr. In contrast, the Amazonian slopes show higher values of precipitation towards the foothills of the Eastern Cordillera, with observed values up to 6,060 mm/yr at the Reventador station (Fig. 1b, easternmost white star). Precipitation values are highly contrasted below 2,500 m a.s.l. and can reach up to 4,000 mm/yr, precipitation values within the range 400−1,500 mm/yr are found in the 2,500−3,500 m a.s.l. range, whereas precipitation values within the 600−3,500 mm/yr range are observed above 3,500 m a.s.l. (Fig. S-2).

An interesting feature of the Amazonian slopes is the strong spatial variation in precipitation over short horizontal distances, particularly on the eastern ridge of the Andes (Fig. 1b, Cordillera Central ridge). Fig. 1c shows a profile that crosses several prominent orographic features in the study zone. The maximum of precipitation in the profile section Y-Z is 3660 mm/yr and, at a nearby station, the precipitation decreases to 989 mm/yr (i.e. a 73 % decrease) within a horizontal distance of 8 km. These values represent an exceptional spatial variation of 330 mm/yr/km in comparison with spatial variations of 190 mm/yr/km identified in the rainfall hotspots in the Central Andes (Espinoza et al., 2015) and 68 mm/yr/km in the Himalayan region (Immerzeel et al., 2014). In addition, the evaluation of altitudinal linear gradients that follow preferential orographic paths such as catchment axes (e.g. Trachte et al., 2018) or swath profiles (e.g., Andermann et al., 2011) shows a positive annual gradient of 200 mm per km of altitude in the section X-Y.

3.2. *Diurnal and seasonal circulations*

The regional atmospheric circulation influencing the zone is dominated by easterly winds (Fig. 2a–d), suggesting that most of the moisture is transported from the Atlantic Ocean and the Amazon basin. Northwesterly winds (Fig. 2a, b) transport moisture from the eastern Pacific mainly in December-May since winds are weak in June-August and September-October seasons (Fig. 2c, d). Maxima of easterly winds are observed during the June-August season (Fig. 2c) that are impinged by the Cordillera and can transport moisture upslope by main river valleys. Indeed, in June-August, the maxima of precipitation of the Amazon basin are displaced to its northwestern part, very close to the Ecuadorian Amazonia (Espinoza et al., 2009).

Analysing the vertical structure of the atmosphere on diurnal time scales, a clear contrast of upslope (Fig. 2e–h) and downslope (Fig. 2i–l) winds are observed between daytime and nighttime during all the months at both sides of the Cordillera. On the other hand, the vertical structure of moisture varies slightly throughout the year during daytime and nighttime in the Amazon and the Ecuadorian lowlands close to the Pacific coast (hereafter referred to as Pacific plains), as is typical of tropical regions. However, more humid conditions are distinguished at low-pressure levels on the Amazon compared to the Pacific plains. The details of circulation in the inter-Andean valley are not observable at the resolution of the data from ERA5.

The moisture available during December-May in the Pacific plains is transported upslope towards the inter-Andean valley, probably by thermal-induced breezes and mechanical uplift (Fig. 2e, f). Interestingly, at nighttime in January (Fig. 2i), unlike the other months, upslope moisture transport persists, suggesting that mechanical uplift is dominant. On the other hand, moisture in the Amazon plains is continuously transported towards the Cordillera by low- and mid-level easterlies. Easterly winds are intensified in July (Fig. 2g, k), and the wind pattern suggests a significant moisture transport towards the Amazonian slope during both daytime and nighttime. However, the atmospheric subsidence observed in the mid-levels (500−600 hPa) acts as a barrier that causes moisture to accumulate on the Amazonian slope, with dry conditions prevailing in the highlands.

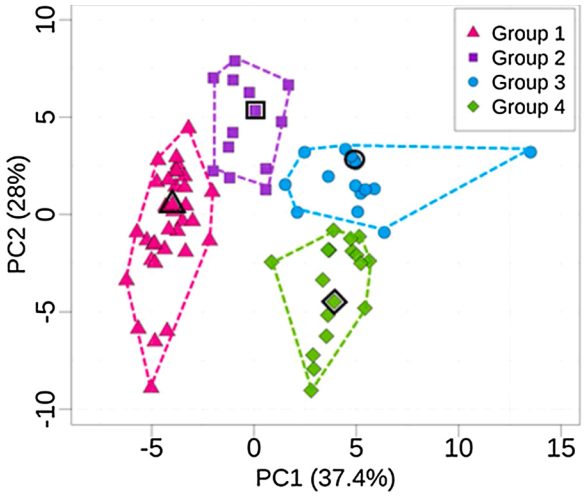

Fig. 3. Representation of the four groups of diurnal cycles in the reduced principal components space PC2-PC1 estimated via PAM using the 6 h-dataset. The medoids are shown in black markers. The convex hull for each group is also displayed to sketch the compactness of each group. The associated station codes are displayed in Fig. S-4.

3.3. Diurnal cycle of precipitation

According to the criteria defined in Section 2.4, clustering the 6 h-dataset in four groups is accurate to regionalize the diurnal cycle of the study zone. The two first principal components (PC1-PC2) for the 6 h-dataset, which represent 37.4 % and 28 % of the total variance, respectively, satisfy the criteria of non-overlapping convex hulls of the groups (Figs. 3, S-3–S-5).

Based on this result, four dominant diurnal cycles are clearly depicted in the study zone. These groups present a spatial distribution in the NW-SE direction, perpendicular to the axis of the Cordillera (Figs. 4a and S-6). Group 1 gathers most of the stations (34 stations) located on Flanks A, B, and C. Group 2 gathers 13 stations mostly on Flank C. Group 3 gathers 15 stations near the Cordillera Central ridge and is embedded with stations from Group 4, demonstrating the effect of the Andes-Amazon transition zone. Finally, Group 4 gathers 18 stations, mostly on the eastern side of the Cordillera Central ridge.

In order to identify the finest features of the diurnal cycle grouped using the 6 h-dataset, the following description is provided using

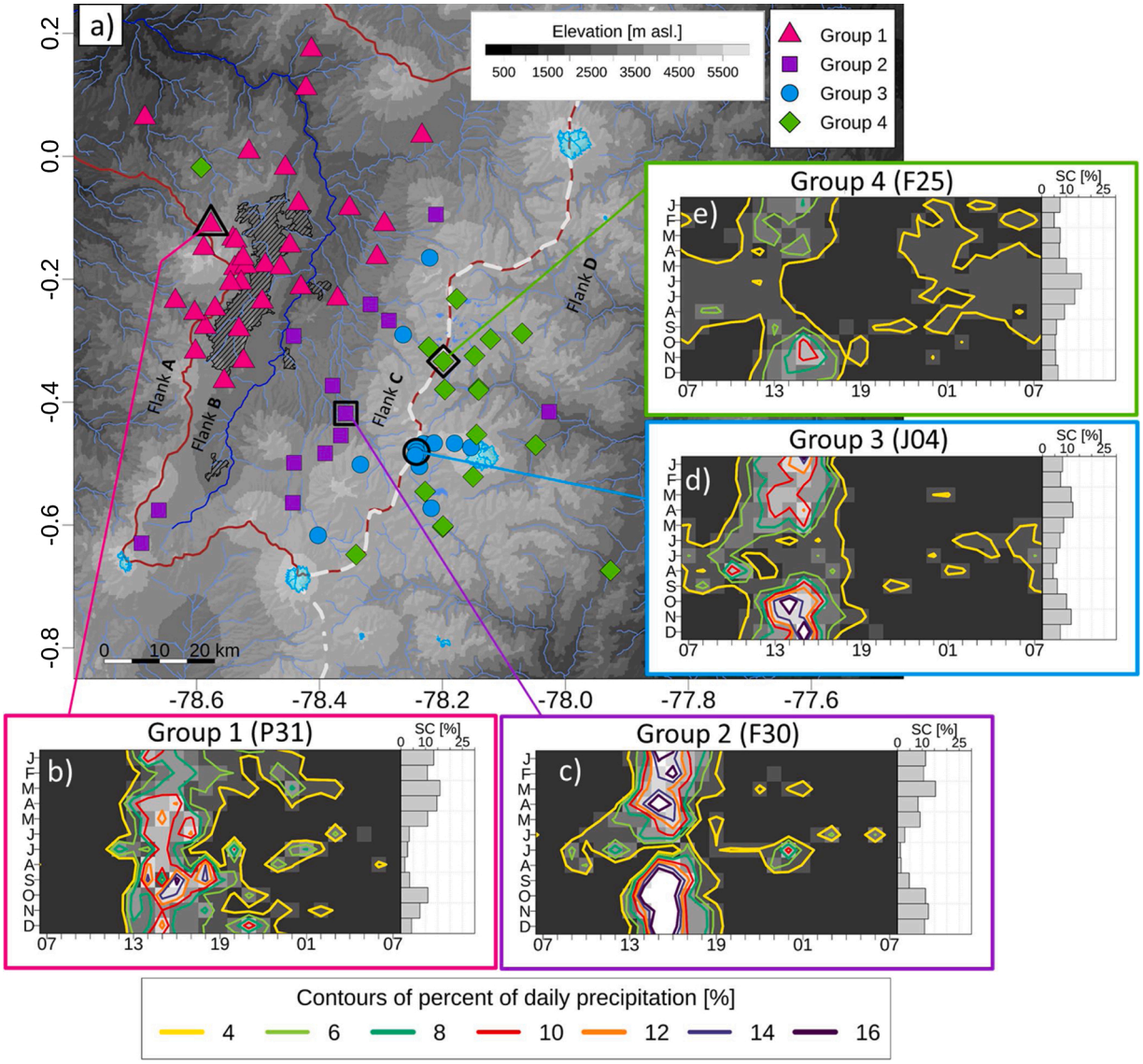

Fig. 4. a) Spatial distribution of the groups of diurnal cycles and the medoid (bold shapes) of each group. Diurnal and seasonal cycle of medoids for b) Group 1, c) Group 2, d) Group 3, and e) Group 4. Diagrams b)-e) are made up of two panels. The panel on the right-hand side, with horizontal grey bars, is the seasonal cycle expressed as the monthly percentage of mean annual precipitation SC [%], and the diagram on the left-hand side is the mean monthly diurnal cycle expressed as a percent of the daily precipitation. The contours represent the percent of total daily precipitation throughout the seasonal cycle. The yellow contour is fixed at a minimum value of 4% which roughly represents the percentage of precipitation within one day with a uniform precipitation concentration. This means that, above this value, the diurnal cycle can be clearly distinguished. The diagrams should be carefully interpreted since a high precipitation concentration is not necessarily related to high precipitation intensities.

the 1h-dataset for the diurnal cycle where seasonal shifts and diurnal and semidiurnal cycles can be recognized (Fig. 4). For the sake of convenience, we define the diurnal cycle as occurring between 07:00-07:00 LT (GMT-5) in order to be consistent with the regional literature (e.g. Poveda et al., 2005; Bedoya et al., 2019). The medoids (Fig. 4b–e) derived from the 6 h-dataset are therefore the dominant diurnal cycles found in the study zone and exhibit the following features with regards to phase (timing):

A) Group 1 (Fig. 4b) is characterized by daytime precipitation and concentrates precipitation in the afternoon, around 13:00−19:00 LT throughout the year, with higher concentrations during April-December. During February-April and November-December, precipitation is also observed in the night with precipitation occurring until 02:00 LT. During July-August, low precipitation values are also observed in the night, around 00:00−01:00 LT.

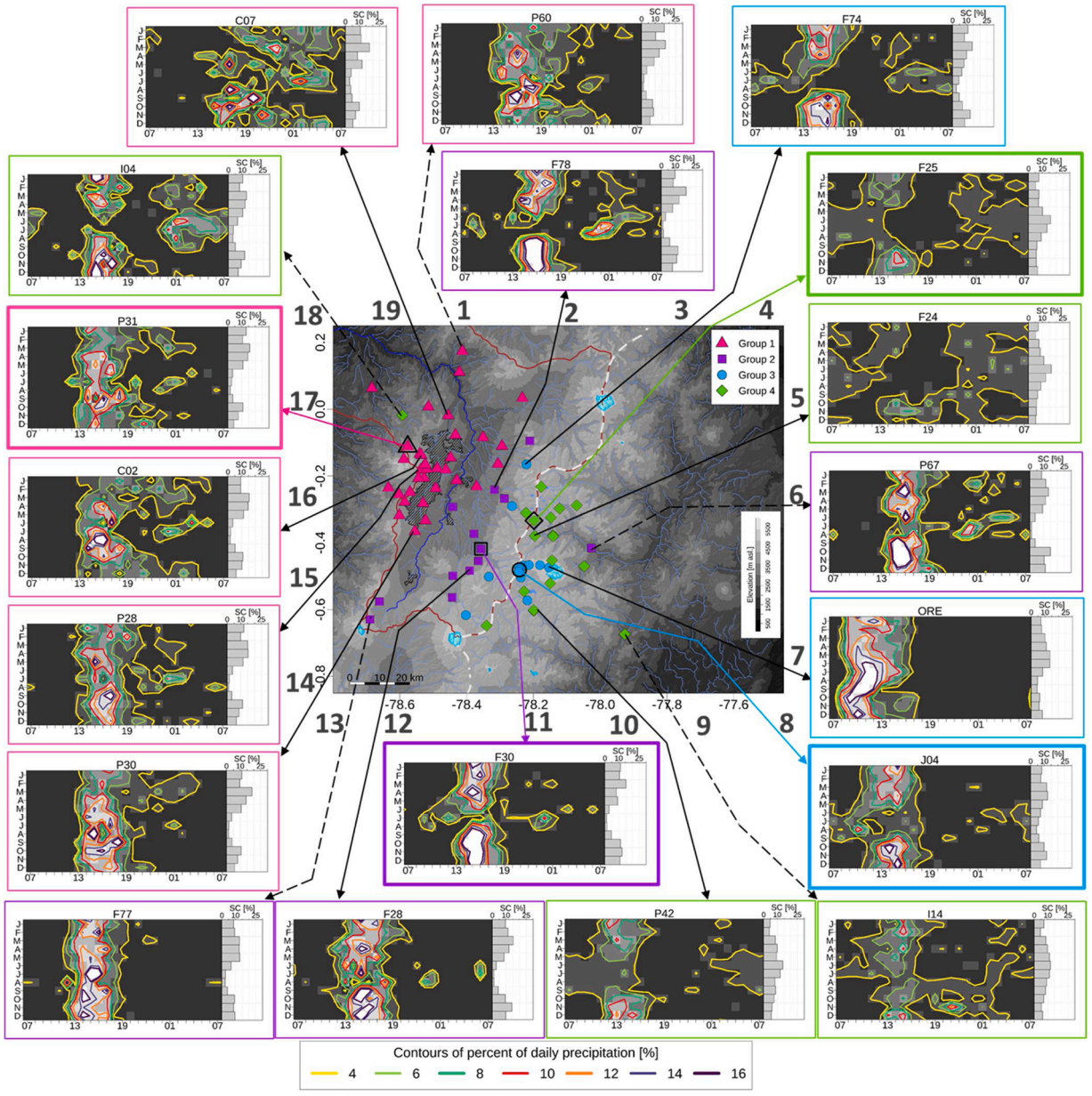

Fig. 5. Same as in Fig. 4 but with the diurnal and seasonal cycle for 19 selected stations. The inner map shows Groups 1-4 and their respective medoids (bold shapes) estimated via the PAM method using the 6 h-dataset. The selection of the stations is based on the PAM method: 11 medoids recommended by the gap statistic performing PAM on the 1h-dataset (black solid arrows), four medoids estimated from the 6 h-dataset (coloured solid arrows) and five manually chosen stations (black dashed arrows). The missing 11th black solid arrow is the same arrow for station J04 (Arrow 8).

B) Group 2 (Fig. 4c) is characterized by a high concentration of precipitation in the afternoon, around 13:00−19:00 LT throughout the year. In particular, in the September-March season, 100 % of the precipitation is observed during 13:00−19:00 LT, with peaks around 15:00−16:00 LT. In June-August, precipitation is also observed in the morning and night. During this season, precipitation shows a better distribution throughout the day, with a small peak around 01:00 LT. Little or a total absence of precipitation is observed around 01:00−08:00 LT.

C) Group 3 (Fig. 4d) concentrates precipitation around 11:00−18:00 LT throughout the year. During the September-May season, a peak of precipitation is clearly observed around 13:00−16:00 LT. During June-August, precipitation is also observed around 01:00−18:00, with a small peak in the morning, around 10:00−11:00 LT.

D) Group 4 (Fig. 4e), in contrast, is characterized by a low precipitation concentration at any one particular time of day, which means that precipitation is observed most of the day. Precipitation is observed during the night and morning (22:00−12:00 LT), particularly during the April-October season. During the November-March season, precipitation is concentrated around 11:00−18:00 LT, with a small peak around 14:00−16:00 LT.

Fig. 5 presents the results of a sample of the 19 stations systematically selected to reflect the spatial distribution and particularities of the diurnal cycle in the zone. The medoids (Fig. 5, arrows 4, 8, 11 and 17) are the representative diurnal cycles of the zone, as demonstrated by the similarity of the diurnal and seasonal patterns present in the sample for each group: Group 1 (Fig. 5, arrows 1, 14, 15, 16, 17 and 19), Group 2 (Fig. 5, arrows 2, 6, 11, 12 and 13), Group 3 (Fig. 5, arrows 3, 7 and 8) and Group 4 (Fig. 5, arrows 4, 5, 9 and 10).

Fig. 5 also shows that there is not a common pattern in the diurnal cycle for the sample of the 19 stations; however, given the variety observed in the diurnal cycles, it is worth mentioning certain aspects: i) for some stations, diurnal cycles are unimodal (diurnal) throughout the year (e.g. Fig. 5, arrows 7 and 13); ii) for others, diurnal cycles switch from a unimodal (diurnal) to bimodal pattern (semi-diurnal) throughout the year (e.g. Fig. 5, arrows 2 and 18); iii) very similar patterns exist between nearby stations (e.g. Fig. 5, arrows 15, 16 and 17; also arrows 4, 5); iv) the timing of the diurnal maxima is similar for some nearby stations (e.g. Fig. 5, arrows 16 and 17 in April and September, both stations peak at 16:00 LT and 18:00 LT, respectively); and v) a slightly different timing for the diurnal maxima for nearby stations can also occur (e.g. Fig. 5, arrows 15 and 16 in August, the stations peak at 17:00 LT and 15:00−16:00 LT, respectively). An unexpected degree of similarity in is observed for two distal stations (Fig. 5, arrows 6 and 18) that is in disagreement with the general picture of the NW-SE geographical orientation for the diurnal cycle groups (Fig. 5, inner panel). However, these stations still show similarities, either in the diurnal pattern alone (Fig. 5, arrow 18) or in both the diurnal and seasonal patterns (Fig. 5, arrow 6), with the medoids of the groups to which the stations belong.

3.4. Seasonal cycle of precipitation

In Section 3.3, we showed that the diurnal cycles vary throughout the year and that four groups of dominant diurnal cycles were found. To investigate a potential relationship between the diurnal and seasonal cycles, we calculated the average seasonal cycles of

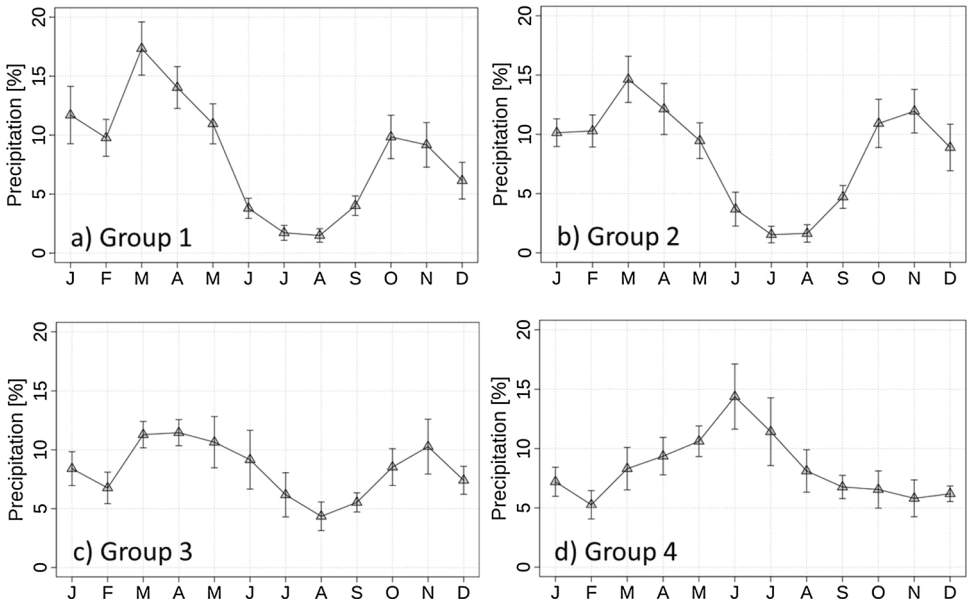

Fig. 6. Mean of the seasonal cycles for the stations within the groups. The triangles indicate the arithmetic mean of the mean monthly precipitation for the stations in each group. The vertical bars show the means +/- one standard deviation calculated with the mean monthly precipitation for the stations. Notice that the seasonal cycles are expressed as the percentage of precipitation [%] of annual totals distributed each month.

precipitation for the stations within each group (Fig. 6). Additionally, the standard deviations for each month were relatively small compared to the mean values. This feature indicates that the grouping of the stations based on the diurnal cycle reflects the associated seasonal cycle well. Keeping in mind the NW-SE orientation of the groups of diurnal cycles, distinct seasonal cycles varying from bimodal (Fig. 6a) to unimodal regimes (Fig. 6d) were found in the study zone.

Groups 1 and 2 (Fig. 6a, b) are associated with bimodal regimes with precipitation maxima in the March-April period and a during the October-November season, separated by two minima around the solstices in the July-August and December-January periods. We observed the strongest seasonality in Groups 1 and 2 (the values are up to seven times higher between the rainiest and driest season). However, unlike Group 1, Group 2 shows more constant precipitation during austral summer. Group 3 (Fig. 6c) may also be associated with a bimodal regime; however, the seasonality of the precipitation is weaker. Relative maxima can be identified during the March-May period and in November, and the lowest relative minima occur during the August-September and December-February periods. Finally, Group 4 is unimodal with a rainy season during the May-July period with the peak in June.

In general, the seasonal index (SI) values of the seasonal cycles (Fig. 7) do not fit in the "seasonal" regime as suggested in Table 1 since all SI values are lower than 0.60. The SI values suggest that the seasonality of Groups 1 and 2 is "rather seasonal with a short drier season"; this dry season occurs in July-August (Fig. 6a, b). For Groups 3 and 4, the seasonality is "equable but with a definite wetter season"; this wetter season occurs in September-May(Fig. 6c) and March-August (Fig. 6d), respectively. Furthermore, the median values of the boxplots in Fig. 7 decrease from Group 1 to Group 4, which indicates an eastward weakening of the precipitation seasonality towards an "equable" regime.

3.5. *Contrasting diurnal and seasonal cycles*

The drier seasons identified for Groups 1 and 2 (and the wetter seasons for Groups 3 and 4) demonstrate contrasting features in the patterns for the diurnal cycles, as shown in Fig. 4. Groups 1 and 2 present the same bimodal seasonal cycle, and in the drier season, July-August, the diurnal cycles exhibit different behaviour as well as during the wetter seasons. In Group 1, precipitation is concentrated in the afternoon, whereas, in Group 2, it is concentrated in the morning and night. In Group 3, during the short dry season from June to August, precipitation occurs in the nighttime, whereas precipitation is observed in the daytime during the rest of the year. In contrast, during the wetter season from April to October, Group 4 is characterized by mostly homogeneous precipitation during the morning and night. These findings highlight the complex behaviour of precipitation in the study zone: i) distinct diurnal concentrations of precipitation are observed in both drier and wetter seasons (e.g. Groups 1, 2 and 3); and ii) there is no marked diurnal cycle throughout the year (e.g. Group 4). The detailed diurnal and seasonal cycles of all stations used in this work are provided in the Supplementary Material (Figs. S-7–S-9).

To reconcile the diurnal cycle groups with their spatial distribution, altitude and seasonal cycles, expressed as monthly precipitation (mm/month), we divided the stations by flank, sorting them by altitude (Fig. 8). Fig. 8a presents Flank A and Flank B stations, ordered by descending altitude varying from 4,012 m a.s.l. (station P28 on the Cordillera Occidental ridge) to 1,626 m a.s.l. (station C15 the north-western-most station in the study zone in Fig. 1b). Conversely, Fig. 8b shows the stations on the Flank B sorted by ascending altitude from 1,886 m a.s.l. (station P61, the second northernmost station) to 4,148 m a.s.l. (station F74 on the Cordillera Central ridge) and Fig. 8c shows the stations sorted from 4,850 m a.s.l. (ORE station, the highest station in the study zone and the closest one to the Antizana glacier) to 2,240 m a.s.l. (station I14, the south-eastern-most station).

Fig. 8 clearly shows the marked bimodal seasonal cycle from station P28 (Fig. 8a) to station F26 (Fig. 8b), enclosing the Group 1 and Group 2 stations in the previously identified NW-SE variation of both diurnal and seasonal cycles. Rainfall peaks characterize these stations during the March-April and October-November seasons and a relatively short dry season (July-August) during austral winter. Stations F76 (Fig. 8b) to I14 (Fig. 8c) enclose the Group 3 and Group 4 stations where the precipitation is better distributed throughout

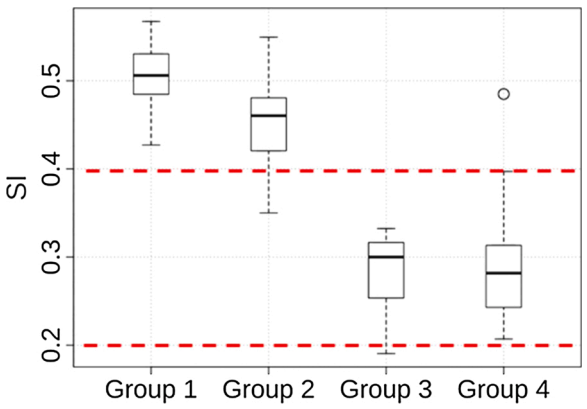

Fig. 7. Boxplots of the Seasonal Index (SI) calculated for the stations within Groups 1-4. The red dashed lines are thresholds used to interpret the SI value as per (Walsh and Lawler, 1981). The boxplots show the median, first and third quartile. The top whiskers are the smaller of two values (and vice versa- the bottom whiskers are the larger of two values): the maximum (minimum) value and the third (first) quartile +(-) 1.5 times the interquartile range. The circle represents one outlier.

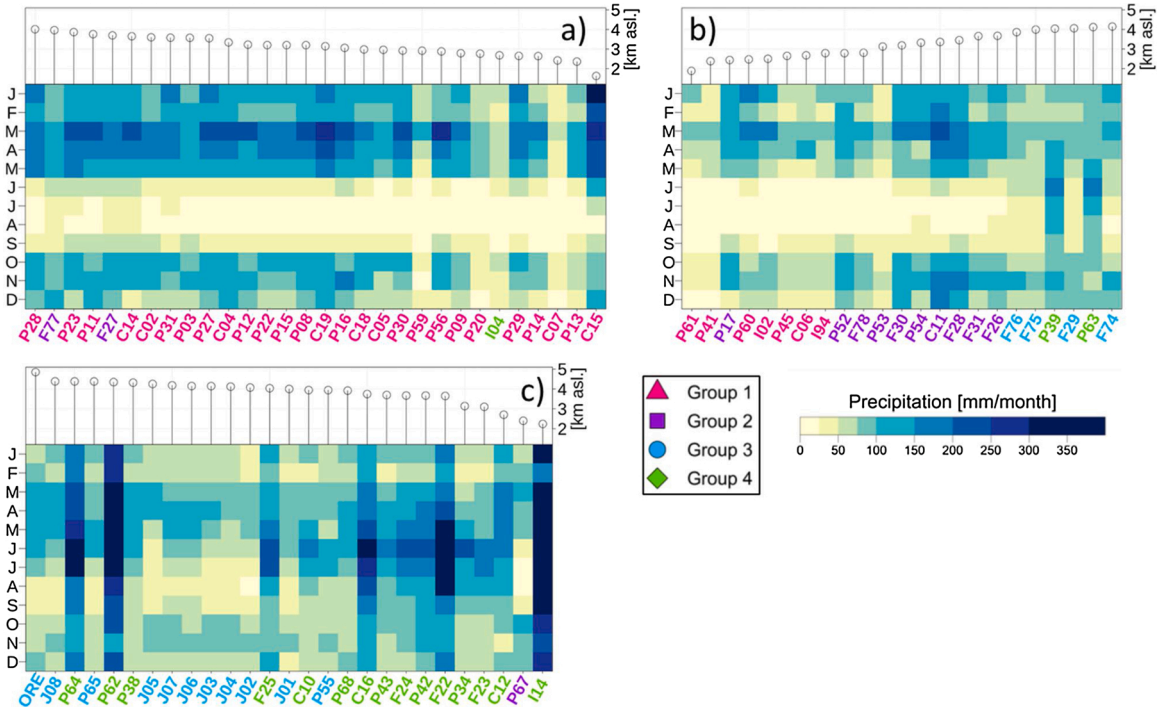

Fig. 8. Mean monthly precipitation of stations during 2014-2019, ordered by a) descending b) ascending c) descending elevation. The panels contain stations located in a) Flanks A and B, b) Flank C, and c) Flank D. The upper panels represent the altitude of each station. The horizontal distance between the stations is not maintained. The colors of the labels on the X-axis indicate the group of each station that are spatially displayed in Fig. S-6.

the year and a peak during austral winter is observed in the Group 4 stations (green labels). The situation of Group 3 and Group 4 in the NW-SE direction is more heterogeneous than Groups 1 and 2, which is explained by the strong spatial gradient that characterizes the Andes-Amazon transition region (e.g. Laraque et al., 2007; Espinoza et al., 2009; Junquas et al., 2018)

4. Discussion

Our results refine the assessment of the coherence among the diurnal and seasonal cycles of precipitation identified by the most recent comparable studies in the tropical Andes using precipitation stations (Poveda et al., 2005; Bedoya et al., 2019). This coherence is clustered in groups of diurnal and seasonal cycles varying spatially in the NW-SE direction, in agreement with the prominent large-scale wind direction (Fig. 2). This is the classical picture of orographic precipitation in mountain ranges where the orography and diurnal thermal contrast modulate the regional-scale diurnal circulation (Roe, 2005; Bendix et al., 2006b; Junquas et al., 2018). In addition, we identify the concomitant spatial variation of both the diurnal and seasonal cycles of precipitation in the study region, which has not yet been reported in previous studies of the equatorial Andes. These results may slightly vary when using different clustering methods and different measures of dissimilarity while performing PAM, but the NW-SE spatial variation remains unaltered.

4.1. Atmospheric dynamics related to the diurnal and seasonal cycles

Key findings emerged regarding the diurnal and seasonal patterns and the related local-regional scale processes driving precipitation. Over seasonal time scales, our findings are consistent with previous work carried out in Ecuador (e.g. Laraque et al., 2007; Ballari et al., 2018; Tobar and Wyseure, 2018; Ilbay-Yupa et al., 2021) and are in line with the regional circulation (Fig. 2). The identified Groups 1 and 2 in the inter-Andean valley are bimodal with peaks in the March-April and October-November seasons. In addition, in Groups 1 and 2, the results clearly show a more significant peak in March-April than in October-November, which could be linked to the spatial proximity of the stations in the groups to the Pacific coast, where a unimodal maximum prevails during austral autumn (see the Section 2.1 and references therein). This behaviour is particularly pronounced for Group 1, which includes the most western stations.

The weak seasonality of Group 3 (relative peaks observed in March-May and November), situated more to the east, could be explained by a weaker influence of the coastal regime and a greater influence of the bimodal Amazonian regime, which entersthe eastern Cordillera westward through the main river valleys (e.g. Campozano et al., 2016, 2018; Tobar and Wyseure, 2018). Whereas these three groups clearly show inter-Andean valley regimes, with different influences of the coastal (western) and Amazonian

(eastern) regimes, Group 4 shows a very distinctive unimodal regime, with a peak in austral winter and maxima in June. This regime has been described in the literature as a particularity of some stations on the eastern slope of the Andes and valleys connected to the Amazonian plains (e.g. Laraque et al., 2007), where the orographic barrier effect of the Andes block strongly the easterlies.

The blocking effect is more pronounced in austral winter, when mid-level moist easterly winds are stronger and oriented perpendicular to the Cordillera (Bendix et al., 2006a; Laraque et al., 2007). However, as has been found in previous studies using data from stations in the eastern Ecuadorian Cordillera, the easterlies' influence and the associated blocking process can show strong local variations. Therefore, the seasonal cycle of nearby stations can be affected differently by this process, depending on the characteristics of their locations (i.e. slope or aspect), which define if they are leeward or windward. Consequently, a bimodal regime is also found on the Amazon slope (e.g. Fig. 5, station marked by arrow 6) due to inter-valley locations sheltered from the influence of easterlies (Campozano et al., 2016). This explains the strong spatial gradient in the eastern Cordillera, characteristic of the Andes-Amazon transition region.

The spatial variability in the diurnal maxima, even in nearby stations, seems to be determined by the stations' local topography and windward and leeward configurations. Afternoon precipitation observed in the inter-Andean valley throughout the year (Groups 1 and 2) appears to be mainly related to local convection and induced thermal upslope breezes, explaining the higher annual precipitation close the Cordillera ridges than in the valley. Nevertheless, the nocturnal precipitation of Group 1 can be attributed to the advected moisture from the Amazon rainforest during seasons (March-April and October-November) with high convective activity. In the eastern foothills of the Andes, nocturnal convective systems are more frequent than daytime convective systems (Campozano et al., 2018). The local-scale katabatic winds flowing towards the Amazon rainforest due to nocturnal divergence over mountains interact with the warm and moist air of the Amazon rainforest, inducing compressional lifting and causing nocturnal cloud clusters called the Andes-occurring system (AOS) rain band (Bendix et al., 2006a). The dynamics of the AOS may explain the nocturnal precipitation at the stations on the Amazon slope that partly changes to morning precipitation as the AOS are transported eastward to the Cordillera. This complex interaction of local-to-regional atmospheric processes in the Andes-Amazon transition zone could be responsible for the nocturnal and morning peaks observed in Groups 2, 3 and 4.

It should be noted that the present study has not examined the inter-annual (e.g. ENSO) or intra-seasonal variability (e.g. MJO) of the diurnal cycle. In the Colombian Andes, Poveda et al. (2005) found that these modes of variability only modulate the amplitude of the diurnal cycle and do not alter its phase. Nevertheless, it is important to bear in mind that the diurnal and seasonal cycles investigated in this six-year period could be capturing stationary conditions. However, they are regular and preserve their periodicity over long-term scales (Poveda et al., 2005; Espinoza et al., 2020; Arias et al., 2021). The seasonal cycle of precipitation seems to exert an important role in the east-west gradient of greening in the zone (Haro-Carrión et al., 2021). We show that in the eastern part of the Andes, the seasonal cycle of greening identified by Haro-Carrión et al. (2021) is weak as the seasonal cycle of precipitiation. In the inter-Andean valley, the seasonal cycle of greening peaking in July-August agrees with the short dry season identified in the zone.

To develop a full picture of the diurnal cycle in the study zone, high-resolution atmospheric modelling is necessary to accurately investigate the regional-to-local interactions that control the diurnal cycle. Quito (2,850 m a.s.l. Fig. 1a), the capital of Ecuador with 2.6 million inhabitants, depends on a complex infrastructure of water intakes and conductions that transport water from high-altitude catchments and the diurnal cycle described in this study could help to better understand hydro-glaciological processes and develop new water management strategies.

5. Conclusions and final remarks

This study analysed the spatial variability of diurnal and annual cycles of precipitation in the equatorial Andes thanks to a dense network of 80 precipitation stations with hourly data, located over an inter-Andean valley and its transition to the Amazon Basin over the 2014–2019 period. The precipitation network allowed us first to identify an exceptionally strong spatial gradient in precipitation, of up to 330 mm/yr/km. Using cluster analysis, we identified, for the first time, groups of stations varying spatially in the NW-SE direction over this region with complex topography which display concomitant diurnal and seasonal variations of precipitation. In the western part of the study area, the seasonal cycles of Groups 1 and 2 are bimodal and typical of equatorial inter-Andean valleys with precipitation maxima in the March-April and October-November seasons and one short drier season in July-August. Conversely, in the eastern part, Group 3 presents a weak bimodal seasonal cycle with relative maxima also in March-April and October-November. Finally, Group 4 is unimodal, with a maximum in June. It is crucial to notice that distinct diurnal cycles are observed in both drier and wetter seasons of Groups 1, 2 and 3; and no marked diurnal cycle is observed in any part of the year in Group 4. Furthermore, Groups 3 and 4 are the most spatially heterogeneous in annual precipitation and diurnal cycles. This local-scale analysis based on precipitation stations agrees with the diurnal and seasonal regional circulation observed in reanalysis (ERA5). The findings of this work complement those of earlier studies in the Tropical Andes that analysed diurnal cycle over complex topography.

The present study lays the groundwork for future research into the atmospheric physical processes linking diurnal and seasonal precipitation cycles that vary spatially over complex topography. Further studies need to be carried out to validate the hypothesis discussed in this paper since the use of Reanalysis data explains the diurnal and seasonal dynamics of moisture partly. For instance, our results encourage the use of high-resolution atmospheric modelling to identify the interaction of local-to-large scale mechanisms driving the diurnal cycle in the equatorial Andes. More broadly, research is also needed to understand the diurnal cycle along the Andes Cordillera in tropical South America to identify the role of oceanic (Pacific and Atlantic) and land (Amazonian basin) moisture sources involved in diurnal cycle variations. The station-based data set presented in this study stress the need to preserve and make denser the current monitoring network in order to capture the long-term dynamics of the diurnal cycle.

The insights gained in this study may help to understand the functioning of Andean hydro-systems. The estimation of water budgets

in the *Páramo* is currently subject to large uncertainty due to the limited number of precipitation stations. The Eastern Cordillera receives the highest amounts of precipitation and displays a weak seasonal cycle. This homogenous precipitation distributed throughout the year emphasises the role of such environments as water suppliers and regulators. Thus, water management planning should be oriented to generate new strategies to cope with possible future changes in the strength of seasonality. For instance, sub-daily scale processes (like flash floods or glacier melting) could be better characterised using the diurnal cycle of precipitation in a hydroglaciological modelling framework.

CRediT authorship contribution statement

Jean-Carlos Ruiz-Hernández: Conceptualization, Data curation, Formal analysis, Funding acquisition, Investigation, Methodology, Software, Validation, Visualization, Writing - original draft, Writing - review & editing. **Thomas Condom:** Conceptualization, Methodology, Writing - review & editing. **Pierre Ribstein:** Conceptualization, Methodology, Writing - review & editing. **Nicolas Le Moine:** Conceptualization, Writing - review & editing. **Jhan-Carlo Espinoza:** Conceptualization, Methodology, Writing - review & editing. **Clementine Junquas:** Conceptualization, Methodology, Writing - review & editing. **Marcos Villacís:** Conceptualization, Writing - review & editing. **Andrea Vera:** Data curation, Resources. **Teresa Muñoz:** Data curation, Resources. **Luis Maisincho:** Data curation, Resources, Writing - review & editing. **Lenin Campozano:** Writing - review & editing. **Antoine Rabatel:** Writing - review & editing. **Jean-Emmanuel Sicart:** Writing - review & editing.

Declaration of Competing Interest

The authors report no declarations of interest.

Acknowledgements

This study was conducted as part of the International Joint Laboratory GREAT-ICE, a joint initiative of the IRD and universities and institutions in Bolivia, Peru, Ecuador and Colombia. We acknowledge the support of the LabEx OSUG@2020 (Investissement d'Avenir – ANR10 LABX56) with regards to the data provided by the Andean part of the French Service National d'Observation GLACIOCLIM (P. I. Antoine Rabatel, Univ. Grenoble Alpes, IRD, CNRS-INSU). JCR thanks to Secretaría Nacional de Educación Superior, Ciencia, Tecnología e Innovación, SENESCYT for financial support through a PhD scholarship. JCE received the support of the French AMANECER-MOPGA project funded by ANR and IRD (ref. ANR-18-MPGA-0008). We are also grateful to Instituto Nacional de Meteorología e Hidrología (INAMHI) and to EPMAPS-FONAG through the Estación Científica Agua y Páramos (ECAP) for providing the precipitation data. The support received from EPMAPS and FONAG during field work is also acknowledged. JCR is also grateful to Dr Hans Segura for valuable scientific discussions during quarantines and Dr Jai Beeman for revising the manuscript edition.

Appendix A. Supplementary data

Supplementary material related to this article can be found, in the online version, at doi:https://doi.org/10.1016/j.ejrh.2021.100924.

References

Andermann, C., Bonnet, S., Gloaguen, R., 2011. Evaluation of precipitation data sets along the Himalayan front. Geochem. Geophys. Geosystems 12 (7). https://doi.org/10.1029/2011GC003513.

Arias, P.A., Garreaud, R., Poveda, G., Espinoza, J.C., Molina-Carpio, J., Masiokas, M., Viale, M., Scaff ;, L., van Oevelen, P.J., 2021. Hydroclimate of the andes part II: hydro-climate variability and sub-continental patterns. Front. Earth Sci. 8, 666. https://doi.org/10.3389/feart.2020.505467.

Ballari, D., Giraldo, R., Campozano, L., Samaniego, E., 2018. Spatial functional data analysis for regionalizing precipitation seasonality and intensity in a sparsely monitored region: unveiling the spatio-temporal dependencies of precipitation in Ecuador. Int. J. Climatol. 38 (8), 3337–3354. https://doi.org/10.1002/joc.5504.

Bedoya-Soto, J.M., Aristizábal, E., Carmona, A.M., Poveda, G., 2019. Seasonal shift of the diurnal cycle of rainfall over Medellin's Valley, Central Andes of Colombia (1998–2005). Front. Earth Sci. 7 https://doi.org/10.3389/feart.2019.00092.

Bendix, J., Lauer, W., 1992. Die Niederschlagsjahreszeiten in Ecuador und ihre klimady-namische Interpretation (Rainy Seasons in Ecuador and Their Climate-Dynamic Inter-pretation). Erdkunde 2 (1992), 118–134.

Bendix, J., Rollenbeck, R., Göttlicher, D., Cermák, J., 2006a. Cloud occurrence and cloud properties in Ecuador. Clim. Res. 30, 133–147.

Bendix, J., Rollenbeck, R., Reudenbach, C., 2006b. Diurnal patterns of rainfall in a tropical Andean valley of southern Ecuador as seen by a vertically pointing K-band Doppler radar. Int. J. Climatol. 26 (6), 829–846. https://doi.org/10.1002/joc.1267.

Beven, K.J., 2012. Rainfall-runoff ; modelling: The Primer, 2nd ed.

Buytaert, W., Celleri, R., Willems, P., Bièvre, B.D., Wyseure, G., 2006. Spatial and temporal rainfall variability in mountainous areas: a case study from the south Ecuadorian Andes. J. Hydrol. 329 (3), 413–421. https://doi.org/10.1016/j.jhydrol.2006.02.031.

Campozano, L., Célleri, R., Trachte, K., Bendix, J., Samaniego, E., 2016. Rainfall and cloud dynamics in the Andes: a Southern Ecuador case study. Adv. Meteorol. 2016, 3192765 https://doi.org/10.1155/2016/3192765.

Campozano, L., Trachte, K., Célleri, R., Samaniego, E., Bendix, J., Albuja, C., Mejia, J.F., 2018. Climatology and teleconnections of mesoscale convective systems in an Andean Basin in Southern Ecuador: the case of the Paute Basin. Adv. Meteorol. 2018, 1–13. https://doi.org/10.1155/2018/4259191.

Chavez, S.P., Takahashi, K., 2017. Orographic rainfall hot spots in the Andes-Amazon transition according to the TRMM precipitation radar and in situ data. J. Geophys. Res. Atmos. 122 (11), 5870–5882. https://doi.org/10.1002/2016jd026282.

Condom, T., Martínez, R., Pabón, J.D., Costa, F., Pineda, L., Nieto, J.J., López, F., Villacis, M., 2020. Climatological and hydrological observations for the South American Andes: in situ stations, satellite, and reanalysis data sets. Front. Earth Sci. 8 https://doi.org/10.3389/feart.2020.00092.
de Angelis, C.F., Mcgregor, G.R., Kidd, C., 2004. A 3 year climatology of rainfall character-istics over tropical and subtropical South America based on tropical rainfall measuring mission precipitation radar data. Int. J. Climatol. 24 (3), 385–399. https://doi.org/10.1002/joc.998.
Espinoza, J.C., Ronchail, J., Guyot, J.L., Cochonneau, G., Naziano, F., Lavado, W., De Oliveira, E., Pombosa, R., Vauchel, P., 2009. Spatio-temporal rainfall variability in the Amazon basin countries (Brazil, Peru, Bolivia, Colombia, and Ecuador). Int. J. Climatol. 29 (11), 1574–1594. https://doi.org/10.1002/joc.1791.
Espinoza, J.C., Lengaigne, M., Ronchail, J., Janicot, S., 2012. Large-scale circulation pat-terns and related rainfall in the Amazon Basin: a neuronal networks approach. Clim. Dyn. 38 (1), 121–140. https://doi.org/10.1007/s00382-011-1010-8.
Espinoza, J.C., Chavez, S., Ronchail, J., Junquas, C., Takahashi, K., Lavado, W., 2015. Rainfall hotspots over the southern tropical Andes: spatial distribution, rainfall intensity, and relations with large-scale atmospheric circulation. Water Resour. Res. 51 (5), 3459–3475. https://doi.org/10.1002/2014WR016273.
Espinoza, J.C., Garreaud, R., Poveda, G., Arias, P.A., Molina-Carpio, J., Masiokas, M., Viale, M., Scaff ;, L., 2020. Hydroclimate of the Andes part I: main climatic features. Front. Earth Sci. 8 https://doi.org/10.3389/feart.2020.00064.
Favier, V., Wagnon, P., Chazarin, J.-P., Maisincho, L., Coudrain, A., 2004. One-year measure-ments of surface heat budget on the ablation zone of Antizana Glacier 15, Ecuadorian Andes. J. Geophys. Res. Atmos. 109 (D18) https://doi.org/10.1029/2003JD004359.
Figueroa, M., Armijos, E., Espinoza, J.C., Ronchail, J., Fraizy, P., 2020. On the relationship between reversal of the river stage (repiquetes), rainfall and low-level wind regimes over the western Amazon basin. J. Hydrol. Reg. Stud. 32, 100752 https://doi.org/10.1016/j.ejrh.2020.100752.
Garreaud, R.D., 2009. The Andes climate and weather. Adv. Geosci. 22, 3–11. https://doi.org/10.5194/adgeo-22-3-2009.
Giles, J.A., Ruscica, R.C., Menéndez, C.G., 2020. The diurnal cycle of precipitation over South America represented by five gridded datasets. Int. J. Climatol. 40 (2), 668–686. https://doi.org/10.1002/joc.6229.
González-Zeas, D., Rosero-López, D., Walter, T., Flecker, A., Lloret, P., De Bièvre, B., Condom, T., Osorio, R., Dangles, O., 2019. Designing eco-friendly water intake portfolios in a tropical andean stream network. Water Resour. Res. 55 (8), 6946–6967. https://doi.org/10.1029/2019WR025190.
Guo, J., Zhai, P., Wu, L., Cribb, M., Li, Z., Ma, Z., Wang, F., Chu, D., Wang, P., Zhang, J., 2014. Diurnal variation and the influential factors of precipitation from surface and satellite measurements in Tibet. Int. J. Climatol. 34 (9), 2940–2956. https://doi.org/10.1002/joc.3886.
Halladay, K., Malhi, Y., New, M., 2012. Cloud frequency climatology at the Andes/Amazon transition: 1. Seasonal and diurnal cycles. J. Geophys. Res. Atmos. 117 (D23) https://doi.org/10.1029/2012jd017770 n/a–n/a.
Haro-Carrión, X., Waylen, P., Southworth, J., 2021. Spatiotemporal changes in vegetation greenness across continental Ecuador: a Pacific-Andean-Amazonian gradient, 1982–2010. J. Land Use Sci. 16 (1), 18–33. https://doi.org/10.1080/1747423X.2020.1866705.
Hersbach, H., Bell, B., Berrisford, P., Hirahara, S., Horányi, A., Muñoz-Sabater, J., Nicolas, J., Peubey, C., Radu, R., Schepers, D., Simmons, A., Soci, C., Abdalla, S., Abellan, X., Balsamo, G., Bechtold, P., Biavati, G., Bidlot, J., Bonavita, M., et al., 2020. The ERA5 global reanalysis. Q. J. R. Meteorol. Soc. 146 (730), 1999–2049. https://doi.org/10.1002/qj.3803.
Ilbay-Yupa, M., Lavado-Casimiro, W., Rau, P., Zubieta, R., Castillón, F., 2021. Updating regionalization of precipitation in Ecuador. Theor. Appl. Climatol. 143 (3–4), 1513–1528. https://doi.org/10.1007/s00704-020-03476-x.
Immerzeel, W.W., Petersen, L., Ragettli, S., Pellicciotti, F., 2014. The importance of ob-served gradients of air temperature and precipitation for modeling runoff ; from a glacier-ized watershed in the Nepalese Himalayas. Water Resour. Res. 50 (3), 2212–2226. https://doi.org/10.1002/2013wr014506.
Junquas, C., Takahashi, K., Condom, T., Espinoza, J.-C., Chavez, S., Sicart, J.-E., Lebel, T., 2018. Understanding the influence of orography on the precipitation diurnal cycle and the associated atmospheric processes in the central Andes. Clim. Dyn. 50 (11), 3995–4017. https://doi.org/10.1007/s00382-017-3858-8.
Kaufman, L., Rousseeuw, P.J., 2008. Partitioning Around Medoids (Program PAM). Finding Groups in Data. John Wiley and Sons, Inc, pp. 68–125. https://doi.org/10.1002/9780470316801.ch2.
Konduru, R.T., Takahashi, H.G., 2020. Effects of convection representation and model resolution on diurnal precipitation cycle over the Indian monsoon region: toward a convection-permitting regional climate simulation [e2019JD032150 2019JD032150]. J. Geophys. Res. Atmos. 125 (16), e2019JD032150 https://doi.org/10.1029/2019JD032150.
Kumar, S., Castillo-Velarde, C.D., Valdivia Prado, J.M., Flores Rojas, J.L., Callañaupa Gutier-rez, S.M., Moya Alvarez, A.S., Martine-Castro, D., Silva, Y., 2020. Rainfall char-acteristics in the Mantaro Basin over Tropical Andes from a vertically pointed profile rain radar and in-situ field campaign. Atmosphere 11 (3), 248. https://doi.org/10.3390/atmos11030248.
Laraque, A., Ronchail, J., Cochonneau, G., Pombosa, R., Guyot, J.L., 2007. Heterogeneous distribution of rainfall and discharge regimes in the Ecuadorian Amazon Basin. J. Hydrometeorol. 8 (6), 1364–1381. https://doi.org/10.1175/2007jhm784.1.
Mapes, B.E., Warner, T.T., Xu, M., 2003. Diurnal patterns of rainfall in Northwestern South America. Part III: diurnal gravity waves and nocturnal convection off ; shore. Mon. Weather Rev. 131 (5), 830–844. https://doi.org/10.1175/1520-0493(2003)131<0830:DPORIN>2.0.CO;2.
Marengo, J.A., 2002. The South American low-level jet east of the Andes during the 1999 LBA-TRMM and LBA-WET AMC campaign. J. Geophys. Res. 107 (D20) https://doi.org/10.1029/2001jd001188.
Mitchell, T., Wallace, J., 1996. An observational study of ENSO variability in 1950-78 and 1979-92. J. Clim. 9 (12), 3149–3161.
Montini, T.L., Jones, C., Carvalho, L.M.V., 2019. The South American low-level jet: a new climatology, variability, and changes. J. Geophys. Res. Atmos. 124 (3), 1200–1218. https://doi.org/10.1029/2018jd029634.
Muñoz, P., Orellana-Alvear, J., Willems, P., Célleri, R., 2018. Flash-flood forecasting in an Andean mountain catchment—development of a step-wise methodology based on the random forest algorithm. Water 10 (11). https://doi.org/10.3390/w10111519.
Negri, A.J., 2002. A TRMM-calibrated infrared rainfall algorithm applied over Brazil. J. Geophys. Res. 107 (D20) https://doi.org/10.1029/2000jd000265.
Negri, A.J., Anagnostou, E.N., Adler, R.F., 2000. A 10-yr climatology of Amazonian rainfall derived from passive microwave satellite observations. J. Appl. Meteorol. 39 (1), 42–56. https://doi.org/10.1175/1520-0450(2000)039<0042:AYCOAR>2.0.CO;2.
Oettli, P., Camberlin, P., 2005. Influence of topography on monthly rainfall distribution over East Africa. Clim. Res. 28, 199–212. https://doi.org/10.3354/cr028199.
Oki, T., Musiake, K., 1994. Seasonal change of the diurnal cycle of precipitation over Japan and Malaysia. J. Appl. Meteorol. 33 (12), 1445–1463. https://doi.org/10.1175/1520-0450(1994)033<1445:SCOTDC>2.0.CO;2.
Paccini, L., Espinoza, J.C., Ronchail, J., Segura, H., 2017. Intra-seasonal rainfall variability in the Amazon basin related to large-scale circulation patterns: a focus on western Amazon-Andes transition region. Int. J. Climatol. 38 (5), 2386–2399. https://doi.org/10.1002/joc.5341.
Padrón, R.S., Wilcox, B.P., Crespo, P., Célleri, R., 2015. Rainfall in the Andean Páramo: new insights from high-resolution monitoring in Southern Ecuador. J. Hydrometeorol. 16 (3), 985–996. https://doi.org/10.1175/jhm-d-14-0135.1.
Pouget, J.-C., Proaño, D., Vera, A., Villacís, M., Condom, T., Escobar, M., Goulven, P.L., Calvez, R., 2017. Glacio-hydrological modelling and water resources management in the Ecuadorian Andes: the example of Quito. Hydrol. Sci. J. 62 (3), 431–446. https://doi.org/10.1080/02626667.2015.1131988.
Poveda, G., Mesa, O.J., Salazar, L.F., Arias, P.A., Moreno, H.A., Vieira, S.C., Agudelo, P.A., Toro, V.G., Alvarez, J.F., 2005. The Diurnal cycle of precipitation in the tropical Andes of Colombia. Mon. Weather. Rev. 133 (1), 228–240. https://doi.org/10.1175/MWR-2853.1.
Rau, P., Bourrel, L., Labat, D., Melo, P., Dewitte, B., Frappart, F., Lavado, W., Felipe, O., 2016. Regionalization of rainfall over the Peruvian Pacific slope and coast. Int. J. Climatol. 37 (1), 143–158. https://doi.org/10.1002/joc.4693.
Recalde-Coronel, G.C., Zaitchik, B., Pan, W.K., 2020. Madden–Julian oscillation influence on sub-seasonal rainfall variability on the west of South America. Clim. Dyn. 54 (3), 2167–2185. https://doi.org/10.1007/s00382-019-05107-2.
Roe, G.H., 2005. Orographic precipitation. Annu. Rev. Earth Planet. Sci. 33 (1), 645–671. https://doi.org/10.1146/annurev.earth.33.092203.122541.
Rollenbeck, R., Bendix, J., 2011. Rainfall distribution in the Andes of southern Ecuador derived from blending weather radar data and meteorological field observations. Atmos. Res. 99 (2), 277–289. https://doi.org/10.1016/j.atmosres.2010.10.018.
Rossel, F., Cadier, E., 2009. El Niño and prediction of anomalous monthly rainfalls in Ecuador. Hydrol. Process. 23 (22), 3253–3260. https://doi.org/10.1002/hyp.7401.

Saavedra, M., Junquas, C., Espinoza, J.C., Silva, Y., 2020. Impacts of topography and land use changes on the air surface temperature and precipitation over the central Peruvian Andes. Atmos. Res. 234, 104711 https://doi.org/10.1016/j.atmosres.2019.104711.

Segura, H., Junquas, C., Espinoza, J.C., Vuille, M., Jauregui, Y.R., Rabatel, A., Condom, T., Lebel, T., 2019. New insights into the rainfall variability in the tropical Andes on seasonal and interannual time scales. Clim. Dyn. 53 (1), 405–426. https://doi.org/10.1007/s00382-018-4590-4598.

Takahashi, H.G., 2010. Seasonal changes in diurnal rainfall cycle over and around the Indochina Peninsula observed by TRMM-PR. Adv. Geosci. 25, 23–28. https://doi.org/10.5194/adgeo-25-23-2010.

Takahashi, H.G., Yoshikane, T., Hara, M., Takata, K., Yasunari, T., 2010. High-resolution modelling of the potential impact of land surface conditions on regional climate over Indochina associated with the diurnal precipitation cycle. Int. J. Climatol. 30 (13), 2004–2020. https://doi.org/10.1002/joc.2119.

Tibshirani, R., Walther, G., Hastie, T., 2001. Estimating the number of clusters in a data set via the gap statistic. J. R. Stat. Soc. Series B Stat. Methodol. 63 (2), 411–423. https://doi.org/10.1111/1467-9868.00293.

Tobar, V., Wyseure, G., 2018. Seasonal rainfall patterns classification, relationship to ENSO and rainfall trends in Ecuador. Int. J. Climatol. 38 (4), 1808–1819. https://doi.org/10.1002/joc.5297.

Trachte, K., Seidel, J., Figueroa, R., Otto, M., Bendix, J., 2018. Cross-scale precipitation variability in a semiarid catchment area on the Western slopes of the Central Andes. J. Appl. Meteorol. Climatol. 57 (3), 675–694. https://doi.org/10.1175/jamc-d-17-0207.1.

Vázquez-Patiño, A., Campozano, L., Ballari, D., Córdova, M., Samaniego, E., 2020. Virtual control volume approach to the study of climate causal flows: identification of hu-midity and wind pathways of influence on rainfall in Ecuador. Atmosphere 11 (8), 848. https://doi.org/10.3390/atmos11080848.

Vicente-Serrano, S.M., Aguilar, E., Martínez, R., Martín-Hernández, N., Azorin-Molina, C., Sanchez-Lorenzo, A., El Kenawy, A., Tomás-Burguera, M., Moran-Tejeda, E., López-Moreno, J.I., Revuelto, J., Beguería, S., Nieto, J.J., Drumond, A., Gimeno, L., Nieto, R., 2017. The complex influence of ENSO on droughts in Ecuador. Clim. Dyn. 48 (1), 405–427. https://doi.org/10.1007/s00382-016-3082-y.

Vuille, M., Bradley, R.S., Keimig, F., 2000. Climate variability in the andes of Ecuador and its relation to tropical Pacific and Atlantic sea surface temperature anomalies. J. Clim. 13 (14), 2520–2535. https://doi.org/10.1175/1520- 0442(2000)013<2520: CVITAO>2.0.CO;2.

Walsh, R.P.D., Lawler, D.M., 1981. Rainfall seasonality: description, spatial patterns and change through time. Weather 36 (7), 201–208. https://doi.org/10.1002/j.1477-8696.1981.tb05400.x.

WMO, 2007. Guide to the Global Observing System (Third Edition). WMO-No. 488, p. 70.

WMO, 2015. Updated in 2018 Manual on the Global Telecommunication System. Annex III to the WMO Technical Regulations (Third Edition). WMO-No. 386, p. 200.

Yang, G.-Y., Slingo, J., 2001. The diurnal cycle in the tropics. Mon. Weather. Rev. 129 (4), 784–801. https://doi.org/10.1175/1520- 0493.